


## Loss of cold atoms due to collisions with residual gases in free flight in a magneto-optical trap

Jing-feng Xiang(项静峰), He-nan Cheng(程鹤楠), Xiang-kai Peng(彭向凯), Xin-wen Wang(王新文), Wei Ren(任伟), Jing-wei Ji(吉经纬), Kang-kang Liu(刘亢亢), Jian-bo Zhao(赵剑波), Lin Li(李琳), Qiu-zhi Qu(屈求智), Tang Li(李唐), Bin Wang(汪斌), Mei-feng Ye(叶美凤), Xin Zhao(赵鑫), Yuan-yuan Yao(姚媛媛), De-Sheng Lü(吕德胜), Liang Liu(刘亮)

**Citation:**Chin. Phys. B . 2018, 27(7): 073701. **doi:** 10.1088/1674-1056/27/7/073701

Journal homepage: http://cpb.iphy.ac.cn; http://iopscience.iop.org/cpb

**What follows is a list of articles you may be interested in**

---

## Direct loading of atoms from a macroscopic quadrupole magnetic trap into a microchip trap

Jun Cheng(程俊), Jing-fang Zhang(张敬芳), Xin-ping Xu(许忻平), Hai-chao Zhang(张海潮), Yu-zhu Wang(王育竹)

Chin. Phys. B . 2017, 26(3): 033701. **doi:** 10.1088/1674-1056/26/3/033701

## Semi-analytical model for quasi-double-layer surface electrode ion traps

Jian Zhang(张见), Shuming Chen(陈书明), Yaohua Wang(王耀华)

Chin. Phys. B . 2016, 25(11): 113701. **doi:** 10.1088/1674-1056/25/11/113701

## Intense source of cold cesium atoms based on a two-dimensional magneto-optical trap with independent axial cooling and pushing

Jia-Qiang Huang(黄家强), Xue-Shu Yan(颜学术), Chen-Fei Wu(吴晨菲), Jian-Wei Zhang(张建伟), Li-Jun Wang(王力军)

Chin. Phys. B . 2016, 25(6): 063701. **doi:** 10.1088/1674-1056/25/6/063701

## An effective method of accelerating Bose gases using magnetic coils

Lu Hai-Chang, Zhai Yue-Yang, Pan Rui-Zhi, Yang Shi-Feng

Chin. Phys. B . 2014, 23(9): 093701. **doi:** 10.1088/1674-1056/23/9/093701

## Nanoscale guiding for cold atoms based on surface plasmons alongtips of metallic wedges

Wang Zheng-Ling, Tang Wei-Min, Zhou Ming, Gao Chuan-Yu

Chin. Phys. B . 2013, 22(7): 073701. **doi:** 10.1088/1674-1056/22/7/073701

---

# Loss of cold atoms due to collisions with residual gases in free flight in a magneto-optical trap*

Jing-feng Xiang(项静峰)[1,2], He-nan Cheng(程鹤楠)[1,2], Xiang-kai Peng(彭向凯)[1,2], Xin-wen Wang(王新文)[1,2], Wei Ren(任伟)[1], Jing-wei Ji(吉经纬)[1], Kang-kang Liu(刘亢亢)[1], Jian-bo Zhao(赵剑波)[1], Lin Li(李琳)[1], Qiu-zhi Qu(屈求智)[1], Tang Li(李唐)[1], Bin Wang(汪斌)[1], Mei-feng Ye(叶美凤)[1], Xin Zhao(赵鑫)[1], Yuan-yuan Yao(姚媛媛)[1], De-Sheng Lü(吕德胜)[1,†], and Liang Liu(刘亮)[1,‡]

[1] *Key Laboratory of Quantum Optics and Center of Cold Atom Physics, Shanghai Institute of Optics and Fine Mechanics, Chinese Academy of Sciences, Shanghai* 201800, *China*

[2] *University of Chinese Academy of Sciences, Beijing* 100049, *China*

(Received 26 March 2018; revised manuscript received 23 April 2018; published online 25 June 2018)

The loss rate of cold atoms in a trap due to residual gas collisions differs from that in a free state after the cold atoms are released from the trap. In this paper, the loss rate in a cold rubidium-87 atom cloud was measured in a magneto-optical trap (MOT) and during its free flight. The residual gas pressure was analyzed by a residual gas analyzer, and the pressure distribution in a vacuum chamber was numerically calculated by the angular coefficient method. The decay factor, which describes the decay behavior of cold atoms due to residual gas collisions during a free flight, was calculated. It was found that the decay factor agrees well with theoretical predictions under various vacuum conditions.

**Keywords:** atom traps, atomic and molecular collision, residual gas

**PACS:** 37.10.Gh, 34.50.Cx, 07.30.Bx **DOI:** 10.1088/1674-1056/27/7/073701

## 1. Introduction

Progress in laser cooling and trapping of neutral atoms has made it possible to produce samples with a large number of cold atoms.[1] Such samples will be useful for high-resolution spectroscopy, collision measurements, and frequency standards.[2] In a cold atom frequency standard, such as fountain atomic clocks, the number of the detected cold atoms is very important for obtaining high performance. In these systems, the quantum projection noise is inversely proportional to the square root of the number of the detected atoms $N_{\rm at}$. A higher effective number of atoms is required to improve the stability of the clock.[3] On the other hand, cold atom clocks using the Ramsey method[4] require a longer time interval between two $\pi/2$ pulses in order to obtain more narrow linewidths. While the longer time interval may lead to greater loss due to residual gas collisions.

The magneto-optical trap (MOT) is widely used to produce cold atomic samples,[5–7] and the basic connection between the loss rate of a MOT and the background gas pressure has been understood.[8–10] In a relatively shallow trap, such as far off resonance traps and magnetic traps, the corresponding residual gas collision mechanism has also been studied.[11–13] However, few articles have been published on the loss of cold atoms due to collisions with residual gas during a free flight. The cold atom clock operated in a microgravity is proposed to obtain a longer interrogation time, which may narrow the Ramsey linewidth.[14,15] Similarly, the space matter-wave interferometer is designed by using a longer pulse separation time in microgravity environments with the goal of enhancing the sensitivity.[16] The loss of cold atoms due to residual gas collisions may dominate because of their longer free flight time. For cold atoms during free flight, collisions may result in very small scattering angles. This ejects the cold atoms from the cloud, and the theory describing the loss rate due to residual gas collisions needs to be verified for the cold atoms during free flight.

In this paper, a theory connecting the residual gas pressure and the decay of a cold atom cloud in a MOT and during free flight is presented. The residual gas is analyzed using a residual gas analyzer. The stationary molecular flow of a vacuum chamber is also calculated numerically by the angular coefficient method, using the molecular flow module of COMSOL. Experiments are compared with the corresponding theory, and it is found that the experimental results agree well with theoretical predictions. The results are significant, as they verify the reliability of the theory. According to the theory, we can estimate the required vacuum pressure and design the vacuum system accordingly.

*Project supported by the Ministry of Science and Technology of China (Grant No. 2013YQ09094304).

†Corresponding author. E-mail: dslv@siom.ac.cn

‡Corresponding author. E-mail: liang.liu@siom.ac.cn

© 2018 Chinese Physical Society and IOP Publishing Ltd 

## 2. Theory of the loss rate in a MOT and during free flight

The MOT loading and loss process can be described by the following rate equation:[17]

$$\frac{\mathrm{d}N(t)}{\mathrm{d}t} = R - \gamma N(t) - \beta \bar{n} N(t), \tag{1}$$

where $N(t)$ is the number of atoms in the trap, and $R$ is the loading rate of the magneto-optical trap. Normally, $R$ is proportional to the density of the species being trapped, and $\gamma$ is the trap loss in the MOT that is caused by residual gas collisions. $\beta$ is a rate constant for losses due to inelastic two-body collisions within the MOT, and $\bar{n} = \int n(r,t)^2 \mathrm{d}V / \int n(r,t) \mathrm{d}V$. For larger $N$ values, light scattering enforces a constant density $\bar{n}$. In the constant density limit,[17] equation (1) results in an exponential loading curve

$$N(t) = \frac{R}{\Gamma}(1 - \mathrm{e}^{-\Gamma t}), \tag{2}$$

with $\Gamma = \gamma + \beta \bar{n}$ . For smaller $N$, the exponential curve can also be observed when $\gamma \gg \beta \bar{n}$. By fitting a curve such as that shown in Fig. 3, $R$ and the loss rate $\Gamma$ can be determined. It is also found that the measured loading curves are exponential to a good approximation.

On the other hand, the loss rate $\gamma$ can generally be expressed as

$$\gamma = \sum_i n_i \langle \sigma_i v_i \rangle, \tag{3}$$

where the sum is over gas species $i$ in the background vacuum with density $n_i = P_i/(k_\mathrm{B}T)$ according to the ideal gas law, $v_i$ is the gas velocity, and $\sigma_i$ is the collision loss cross section. The brackets represent an average over a Maxwell–Boltzmann distribution at temperature $T$, and the velocity of the trapped atoms can be considered negligible compared to gas velocity $v_i$.

For MOTs, the interaction potential between the ground-state trapped atoms and residual gas species $i$ can be adequately described using the van der Waals form $-C_i/r^6$.[11,17,18] The well depth $D$ of a MOT is on the order of 1 K, and the speed $s$ imparted to the trapped atom can be calculated during the collision using the impulse approximation.[10] A trapped atom with mass $m_0$ will be knocked out of the MOT if $s > v_0$, where $m_0 v_0^2/2 = D$. Moreover, the density $n_i$ can be expressed in terms of the partial pressure $P_i = n_i k_\mathrm{B} T$. For an incident species with mass $m_i$, after being averaged over a Maxwell–Boltzmann distribution at room temperature $T$, the loss rate due to residual gas species $i$ can be expressed as[10,17]

$$\gamma_i \approx 6.8 \frac{1}{(k_\mathrm{B}T)^{2/3}} \left(\frac{C_i}{m_i}\right)^{1/3} (D m_0)^{-1/6} P_i. \tag{4}$$

According to Eq. (4), the MOT loss rate is related to the sixth root of the well depth, and different well depths have a minor influence on the MOT loss rate. It has been found in the results of Dongen[12] that $\gamma_i$ depends only weakly on the well depth $D$; the loss rate differs by about 30% when the well depth ranges from 0.55 K to 2.2 K.

For collisions between the excited state trapped atoms and residual gas (non-alkali-metal species), the loss rate coefficients can be expected to differ by no more than 30% from the ground-state estimates.[17] Moreover, the loss rate due to the collision between the trapped atoms and hot atoms of the same species can be measured by varying the density of the hot atoms.

For relatively shallow traps, such as far off resonance traps[19,20] and magnetic traps,[21] typical well depths range from less than 1 mK to 10 mK. When the scattering angles required to eject atoms from the trap are sufficiently small, a classical small-angle approximation is not valid.[22] The loss rate can be given by

$$\gamma_i = n_i v_\mathrm{r} \int_{\theta_0}^{\pi} 2\pi \sin\theta \, |f(\theta)|^2 \, \mathrm{d}\theta, \tag{5}$$

where $v_\mathrm{r}$ is the relative velocity, $f(\theta)$ is the scattering amplitude, and $\theta_0$ is determined by the well depth.[11]

Similarly, for cold atoms (the temperature of the cold atom cloud is on the order of 1–100 μK) during free flight, very small scattering angles may result in ejection of cold atoms from the cold atom cloud. There is no well depth for cold atoms during free flight, and the collision loss cross section is equal to the total collision cross section and the total collision cross section can be obtained by the optical theorem.[23] The corresponding loss rate is obtained by evaluating Eq. (5) in the limit $\theta_0 \approx 0$,

$$\gamma_i \approx n_i v_\mathrm{r} \sigma(v_\mathrm{r}). \tag{6}$$

In this case, the integral over $\theta$ essentially yields the total cross section, and the total cross section for collisions with a room-temperature residual gas can be evaluated using semi-classical phase shifts for a interaction potential $V(r) = -C_i/r^6$.[11,24] The total cross section is most conveniently obtained using the optical theorem.[23,24] For the interaction potential $-C_i/r^6$, the total cross section between the cold atoms and residual gas species $i$ can be given by

$$\sigma(v_\mathrm{r}) \approx 8.08 \left(\frac{C_i}{\hbar v_\mathrm{r}}\right)^{2/5}. \tag{7}$$

The loss rate should be averaged over the Maxwell–Boltzmann distribution of residual gas speed. The flying velocity of the cold atoms is much smaller than the most probable velocity of the residual gas and can be neglected. In this case, the loss rate can be expressed as

$$\gamma_i \approx 1.05 \frac{u_\mathrm{p} \sigma(u_\mathrm{p})}{k_\mathrm{B} T} P_i, \tag{8}$$

where $u_p = \sqrt{2k_BT/m_i}$ is the most probable velocity of the residual gas. According to Eq. (8), the loss coefficient depends on the residual gas species through $C_i$ and $m_i$. The van der Waals coefficients $C_i$ can be obtained from Arpornthip's work,[17] or they can be calculated using the Slater–Kirkwood formula.[25,26]

**Table 1.** Calculated loss coefficients for collisions between cold Rb atoms and the residual gases. The MOT well depth is 1 K and the residual gas temperature is 300 K. The $C_i$ coefficients are expressed in atomic units and are taken from Ref. [17] or calculated using the Slater–Kirkwood formula. The loss coefficients $\gamma_i/P_i$ in the MOT are calculated by Eq. (4), and the loss coefficients $\gamma_i/P_i$ during free flight are calculated by Eq. (8).

| Species | $C_i$/a.u. | $\gamma_i/P_i$ in a MOT /Pa$^{-1}$·s$^{-1}$ | $\gamma_i/P_i$ during free flight /Pa$^{-1}$·s$^{-1}$ |
|---|---|---|---|
| $H_2$ | 137 | $3.69\times10^5$ | $1.17\times10^6$ |
| He | 35 | $1.86\times10^5$ | $5.51\times10^5$ |
| $CH_4$ | 440 | $2.72\times10^5$ | $1.00\times10^6$ |
| $H_2O$ | 241 | $2.14\times10^5$ | $7.59\times10^5$ |
| $N_2$ | 302 | $1.99\times10^5$ | $7.27\times10^5$ |
| CO | 337 | $2.07\times10^5$ | $7.60\times10^5$ |
| Ar | 278 | $1.72\times10^5$ | $6.32\times10^5$ |
| $CO_2$ | 482 | $2.00\times10^5$ | $7.66\times10^5$ |

## 3. Experimental setup and methods

Experiments were based on the $^{87}$Rb space cold atom clock (SCAC) designed for operating in microgravity. The Ramsey cavity of the SCAC is a ring cavity with four end-end rectangular waveguide cavities, according to the U-type interrogation cavity.[27] The schematic diagram of the experimental setup is shown in Fig. 1. We have developed an ultra-high vacuum (UHV) chamber with $10^{-8}$ Pa background pressure in the Ramsey interaction zone and $10^{-7}$ Pa background pressure in the MOT zone.[28] The design of the UHV chamber includes a vacuum tube, a rubidium base, and a dual-pump system. The vacuum tube includes cooling, selection, interaction, and detection zones, as shown in Fig. 1.

The double-pump system includes an ion pump (TiTan$^{TM}$ 3S ion pump) and getters (St 171/HI/16-10), and the system is used to keep the SCAC vacuum near $5\times10^{-8}$ Pa.[28] The ion pump is connected to the vacuum tube by a flange, as shown in Fig. 1. Two groups of getters are installed at the two ends of the interaction zone, and each group contains 4 getters.[28]

A vacuum valve for UHV and XHV applications makes it possible to connect the ultra-high vacuum system and the external pump group when the space cold atom clock is assembled. The external pump group consists of an ion pump and a residual gas analyzer. As shown in Fig. 1, the residual gas analyzer (RGA100, Stanford Research Systems) is used to measure the partial pressure of different gas species in the ultra-high vacuum. The partial pressure was measured using the residual gas analyzer (RGA), as shown in Fig. 2. The 40 L/s ion pump (VacIon Plus 40, Varian) was used to maintain the vacuum of the system during operation of the residual gas analyzer.

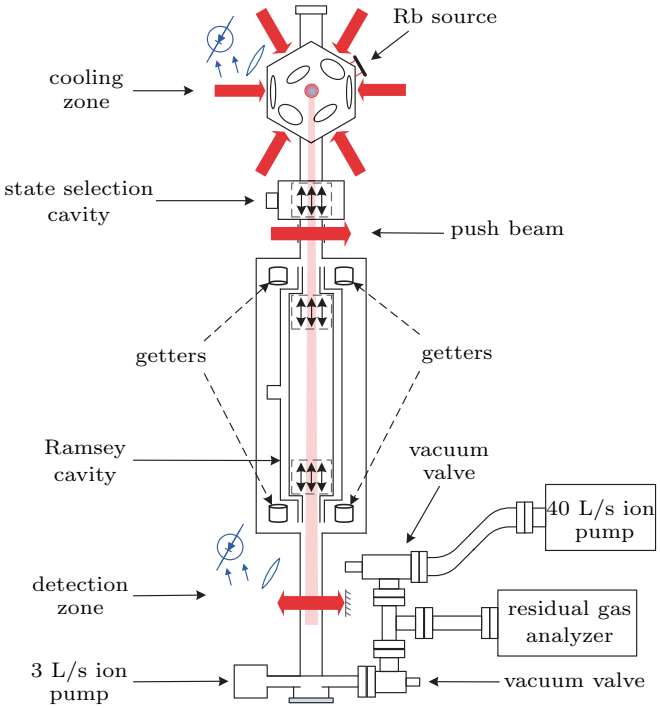



**Fig. 1.** (color online) Schematic of the UHV chamber.

The $^{87}$Rb atoms are stored in an oxygen-free copper cell rather than a rubidium dispenser, which is designed to allow diffusion into the cooling zone. The cell is temperature controlled during the experiment. About $10^8$ Rb atoms can be captured by a compact MOT,[29] which is built with two cooling lasers reflected by the mirrors in the cooling zone. The cooling lasers are red detuned by about 18 MHz to the $|5^2S_{1/2}, F=2\rangle \rightarrow |5^2P_{3/2}, F'=3\rangle$ transition of the $^{87}$Rb D2 line. The repumping laser is operated at a frequency corresponding to the $|5^2S_{1/2}, F=1\rangle \rightarrow |5^2P_{1/2}, F'=2\rangle$ transition. An imaging lens is aligned with the center of the MOT, and the MOT fluorescence is collected with a photodiode. MOT loading experiments were performed by switching AOMs and recording the photodiode current with a digital multi-meter (Agilent 34410A).

The atomic sample is launched by moving molasses, and as a result the cold atoms move towards the state selection cavity at a velocity depending on the frequency difference between the two lasers. In this experiment, cold atoms are launched vertically downward with 1 m/s velocity, and cold atoms have a free flight time of about 300 ms. At the beginning of the flight, the cold atoms are further cooled to about 2 μK in the moving molasses by post cooling.[30,31] The atoms are cooled by tuning the frequency of the cooling lasers from $-2\Gamma$ to $-12\Gamma$ while reducing the power of the cooling lasers asymptotically to zero.[32]

Cold atoms fly through the selection zone, the Ramsey interaction zone, and the detection zone in succession. Once the cold atoms enter the detection zone, $F = 2$ atoms are detected using a standing wave tuned near the $|5^2S_{1/2}, F = 2\rangle \rightarrow |5^2P_{3/2}, F' = 3\rangle$ cycling transition. The TOF signal of the cold atom is sampled and recorded by the control electronics system.

To test the relationship between the vacuum pressure and the loss rate of cold atoms, we varied the background vacuum pressure. As shown in Fig. 1, we used the vacuum valve connected to the 40 L/s ion pump in the external pump group. The flow rate in the vacuum valve can be changed by varying the distance between the valve plate and valve seat. When the valve plate is set to a different distance from the distance where the valve is completely closed, the vacuum valve has a different molecular flow conductance. This changes the effective pumping speed of the 40 L/s ion pump. We recorded the MOT loading process and the TOF signal of the launched cold atoms under different background vacuum pressures.

## 4. Experimental results and analysis

Figure 2 shows the mass spectrum scanned by the analog mode of the RGA, and it is found that hydrogen is the primary residual gas species under a high vacuum or ultra-high vacuum. There are two kinds of vacuum pumps in the vacuum system shown in Fig. 1, which are the ion pump and getter. The two kinds of vacuum pumps have different pumping speeds for different gases.

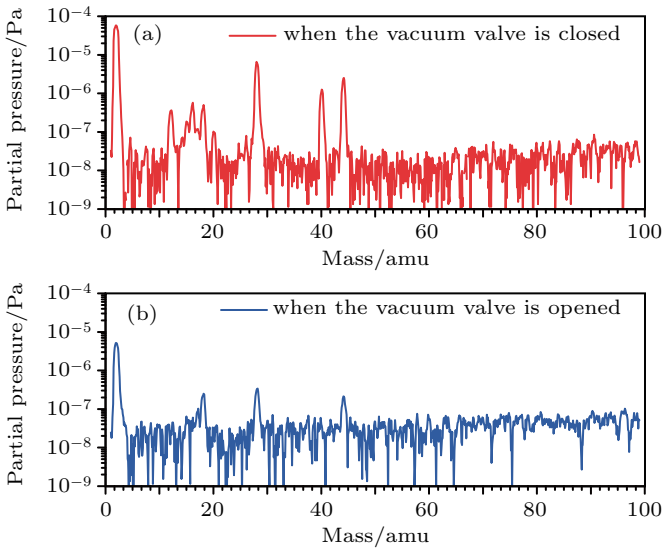



**Fig. 2.** (color online) The mass spectrum measured by RGA up to 99 amu, showing partial pressure (log scale) vs. mass for different conditions: (a) the red line shows partial pressure measurements when the vacuum valve connected to the 40 L/s ion pump is closed; (b) the blue line shows measurements when the vacuum valve is open.

The getter has no pump for rare gases, and the 3 L/s ion pump has a pump speed for these gases. Meanwhile, there is a distance between the ion pump and the RGA, and the effective pumping speed of the 3 L/s ion pump at the RGA position will be further reduced. When the vacuum valve connected the 40 L/s ion pumps is closed, a rare gas (such as argon, methane, and neon) peak appears at the corresponding position.

For hydrogen and other gases (such as nitrogen, carbon monoxide, carbon dioxide, and water), there is a longer distance between the getter and the RGA, and the effective pumping speed of the getter at the RGA position will also be reduced. When the vacuum valve connected to the 40 L/s ion pumps is closed, the partial pressures of these gases at the RGA are increased. As shown in Table 1, the van der Waals coefficient $C_6$ between rubidium and nitrogen is approximate to that between rubidium and carbon monoxide. Because nitrogen and carbon monoxide have the same atomic mass, the loss coefficient for collisions between cold Rb atoms and nitrogen is close to that between cold Rb atoms and carbon monoxide, so we do not distinguish nitrogen from carbon monoxide.

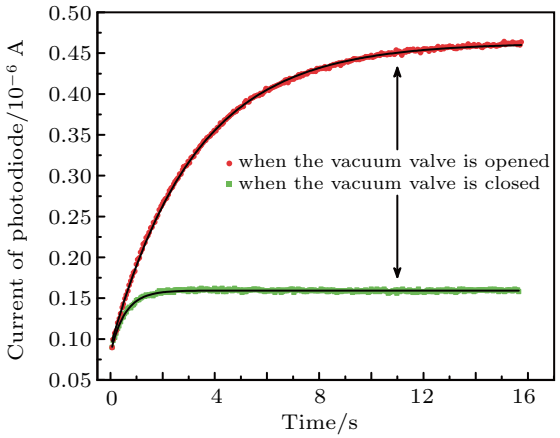



**Fig. 3.** (color online) MOT loading dynamics. The vertical axis shows the photodiode current after switching on the AOMs at time $t = 0$. Data points are the experimentally measured values for the $^{87}$Rb MOT. Red points show measurements when the vacuum valve connected to the 40 L/s ion pump is open, and the green points show measurements when the vacuum valve is closed. The two solid (black) curves are the fit of the experimental data to the exponential form of Eq. (2).

The MOT loading curves are shown in Fig. 3. The red points were measured by recording the photodiode current when the vacuum valve connected to the 40 L/s ion pump was open, and the green points were measured when the vacuum valve connected to the 40 L/s ion pump was closed. The two solid (black) curves are the exponential form of Eq. (2); these curves show an excellent fit to the experimental data. The MOT loss rate when the vacuum valve is closed (green) is greater than the loss rate observed when the valve is open (red). The steady-state atom number of the MOT is also larger when the vacuum valve is open. The difference between the red and green data points is due to the different vacuum environments shown in Fig. 2, and the loss rate due to residual gases is also different. When the valve connected to the 40 L/s

ion pump is closed, the pressure of residual gases rises in the cooling zone.

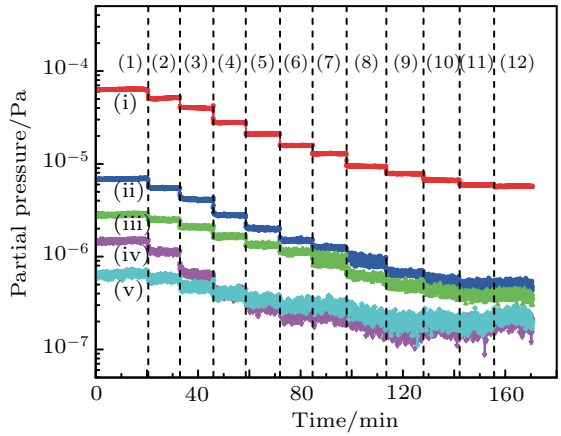



**Fig. 4.** (color online) The data measured by RGA: partial pressure of residual gases ((i) hydrogen, (ii) nitrogen/carbon monoxide, (iii) carbon dioxide, (iv) argon, (v) methane) under different vacuum conditions. The numbers from (1) to (12) indicate the process of varying the vacuum conditions, the number (1) indicates the state of the vacuum valve being closed, and the number (12) indicates the state of the vacuum valve being completely opened.

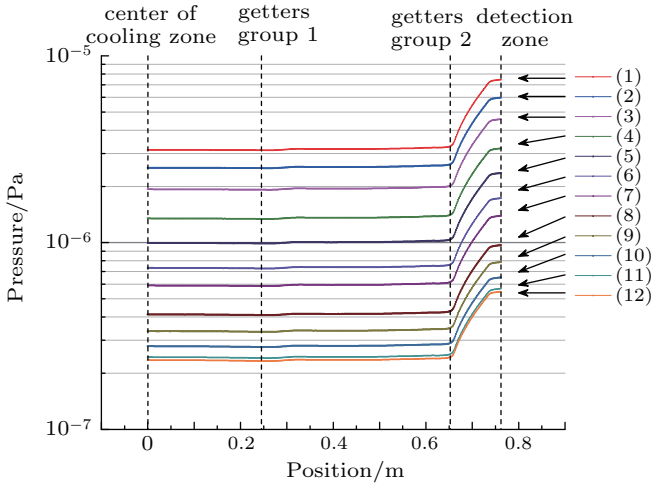



**Fig. 5.** (color online) The typical results of COMSOL: pressure distribution of hydrogen under different vacuum conditions. The numbers from (1) to (12) indicate the process of varying the vacuum conditions, the number (1) indicates the state of the vacuum valve being closed, and the number (12) indicates the state of the vacuum valve being completely opened.

It can be seen from the above that the vacuum valve connecting the 40 L/s ion pump can effectively change the vacuum conditions of the experimental system. In the experiments, we created different vacuum conditions by varying the distance of the valve plate and the valve seat. Figure 4 shows the partial pressure of residual gases measured by RGA when we changed the vacuum conditions. On the other hand, when the RGA is located far away from the cooling zone, the experimental data of RGA cannot be used directly. We used the molecular flow module in COMSOL and the experimental data of RGA to estimate the partial pressure of the cooling zone and the cold atom flight path under the different vacuum conditions. Figure 5 shows pressure distribution of hydrogen under different vacuum conditions, because of the sufficient outgassing of RGA (which is much bigger than outgassing of the vacuum chamber) and the pump speed of getters for hydrogen, the pressure from the detection zone to getters group 2 decreases, while the pressure from getters group 2 to the center of the cooling zone tends to be smooth.

### 4.1. Loss rate due to residual gases in a MOT

Since the MOT captures Rb atoms directly from the background gas in the experiment, the MOT loss rate due to hot Rb atoms in the background should be taken into account. According to Haw's work,[33] the loading rate of the MOT is directly proportional to the density of hot Rb atoms, and the loss rate of the MOT due to the hot Rb atoms is proportional to the density of hot Rb atoms according to Eq. (3). We changed the temperature of the Rb source and recorded the loading curve correspondingly. Figure 6 shows the relationship between the loss rate and loading rate of the MOT. The red points show the experimentally measured values, and the black line is the fitting line for the experimentally measured values. It is important to note that the measurement was performed when RGA was turned off. According to the result of the fitting line, the loss rate of the MOT due to the hot Rb atoms can be estimated when the loading rate of the MOT is known.

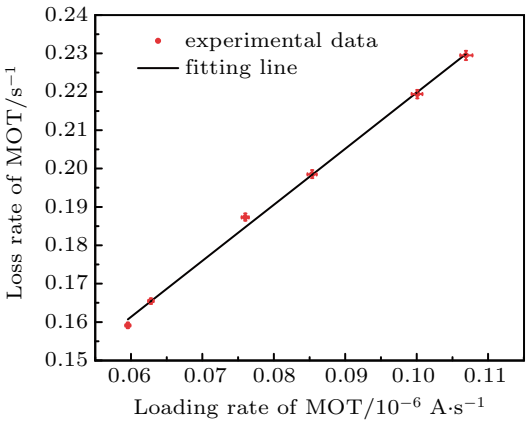



**Fig. 6.** (color online) MOT loss rate versus its loading rate. Red points show the experimentally measured values, and the black line is the fitting line for the experimentally measured values.

Under different vacuum conditions, the MOT loading curves and the TOF signals of the cold atoms were recorded. After simulating the vacuum system by COMSOL, we obtained the pressure distribution of different residual gases under different vacuum conditions (typical in Fig. 5), under which the MOT loading curves and the TOF signals of the cold atoms were recorded. We compared the experimental results with the calculated results (Fig. 7). In Fig. 7, the red data points show the MOT loss rate obtained by fitting the MOT loading curves to the exponential form of Eq. (2). The blue

line shows the calculated loss rate (with loss rate due to hot Rb atom) with residual gases for the 1 K well depth. The black dot line shows the calculated loss rate (with loss rate due to hot Rb atom) with residual gases for the 0.5 K well depth. The black dash line shows the calculated loss rate (with loss rate due to hot Rb atom) with residual gases for the 2 K well depth. The above calculated loss rate is based on the partial pressure obtained from the COMSOL simulation and the theoretical coefficients mentioned above for different gases, and the loss rate due to the hot Rb atom is added. Several major residual gases (hydrogen, nitrogen/carbon monoxide, carbon dioxide, argon, and methane) are considered in these calculations. It can be found that the calculated loss rate of a typical MOT whose well depth is about 1 K (blue line) agrees well with the red points in Fig. 7, which indicates that the results of the partial pressure distribution from COMSOL are credible.

The residual difference is relatively small, mainly from the two-body losses between cold atoms in the MOT and the contribution from other residual gases, such as neon and water. According to the results of Gensemer,[34] the trap-loss collisional rate constant $\beta$ is on the order of $10^{-11}$ cm$^3$·s$^{-1}$ for $^{87}$Rb when the total trap laser intensity is greater than 10 mW/cm$^2$, and trap laser detuning $\Delta$ is $-3\Gamma$ or $-4\Gamma$; the estimated density for our MOT is on the order of $10^9$ cm$^{-3}$ (about $10^8$ atoms in about 0.064 cm$^3$). So the two-body loss $\beta\bar{n}$ between cold Rb atoms in the MOT leads to a small loss rate of the order of $10^{-2}$ s$^{-1}$. According to the curve fitting in Fig. 6, the loss rate is about 0.07 when the density of the hot Rb atoms tends to zero, which indicates that the two-body loss is less than 0.07.

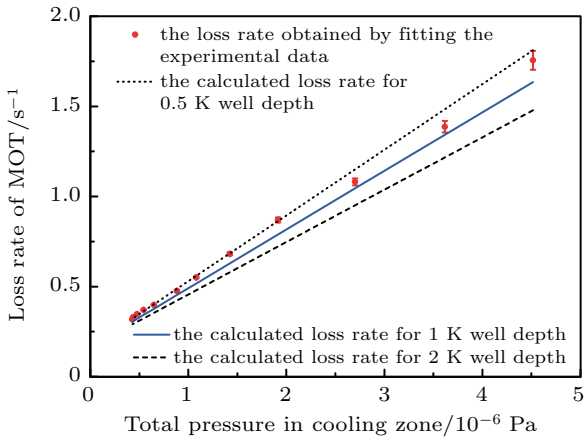



**Fig. 7.** (color online) MOT loss rate versus pressure of residual gases. Red data points show the loss rate obtained by fitting the experimental data for the $^{87}$Rb MOT. The blue line shows the calculated loss rate (with loss rate due to hot Rb atom) with residual gases for the 1 K well depth. The black dot line shows the calculated loss rate (with loss rate due to hot Rb atom) with residual gases for the 0.5 K well depth. The black dash line shows the calculated loss rate (with loss rate due to hot Rb atom) with residual gases for the 2 K well depth.

### 4.2. Loss of cold atoms due to residual gases during free flight

As shown in Fig. 8, the peak height of the TOF signal shows obvious changes in different vacuum conditions, and the number of atoms loaded by the MOT for the same loading time will also be significantly different in different vacuum environments (Fig. 3). What we are interested in is the decay of the cold atom clouds during free flight due to collisions with the residual gas. There are several factors that cause the decay of the cold atom clouds in the experiment. The number of actual detected atoms can be expressed as

$$N_{\rm det} = N_{\rm MOT} \cdot k_{\rm lanuch} \cdot k_{\rm residual-gas} \cdot k_{\rm expansion} \cdot k_{\rm two-body}, \quad (9)$$

$$\frac{N_{\rm det}}{N_{\rm MOT} \cdot k_{\rm lanuch} \cdot k_{\rm expansion} \cdot k_{\rm two-body}} = k_{\rm residual-gas}, \quad (10)$$

where $N_{\rm MOT}$ is the number atoms loaded by the MOT before being launched, $k_{\rm launch}$ represents the fraction of atoms that survive in the process of the launch, $k_{\rm expansion}$ is the decay factor due to the expansion of the atom cloud, $k_{\rm two-body}$ is the decay factor due to two-body losses between cold atoms, and $k_{\rm residual-gas}$ is the decay factor due to the collision with the residual gas in the vacuum system.

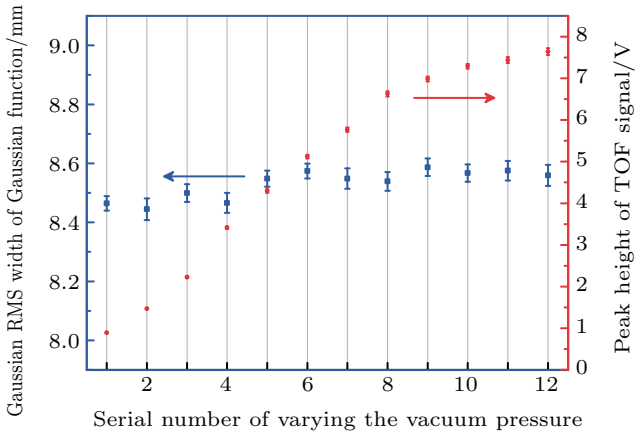



**Fig. 8.** (color online) Results of Gaussian fit for TOF signal of cold atoms. Red points show the peak height of the TOF signal, and the blue points show the Gaussian RMS width of the Gaussian function.

The expansion of cold atomic clouds is mainly affected by the temperature of the cold atoms and their TOF. According to the fitting results of the TOF signal in Fig. 8, the Gaussian RMS width of the TOF signal does not show obvious changes, and the time of flight is about 300 ms. The decay factor due to the expansion of the atom cloud can be assumed to be unchanged, even when the vacuum is changed. Because of the absence of cooling laser beam, the collision cross section between cold atoms may be smaller. According to the SCAC design, copper foam or graphite is fixed between the cooling zone and the state selection zone, as well as between the state selection zone and the Ramsey interaction zone. These materials are used to absorb the background Rb atoms. Meanwhile,

the results reported by Arpornthip[17] seem to indicate that the chamber walls cause a pumping action on the Rb atoms. The decay due to background Rb atoms should be very small during free flight. In summary, it is assumed that only the decay factor due to residual gas changes obviously when we change the effective pumping speed of the 40 L/s ion pump, and the relative decay factor can be expressed as

$$k_{\text{relative}} = \frac{(N'_{\text{det}}/N'_{\text{MOT}})}{(N_{\text{det}}/N_{\text{MOT}})} \approx \frac{k'_{\text{residual-gas}}}{k_{\text{residual-gas}}}. \tag{11}$$

The red points in Fig. 9 represent the decay factor relative to that measured in the experiment when the valve is fully opened. According to the pressure distribution of the cold atom flight path and the theoretical coefficients mentioned above for different gases, we calculate the relative decay factor due to several major residual gases (hydrogen, nitrogen, carbon monoxide, carbon dioxide, argon, and methane). The calculated results are shown with the black dash line in Fig. 9. It can be seen that the experimental relative decay factor agrees well with the calculated relative decay factor.

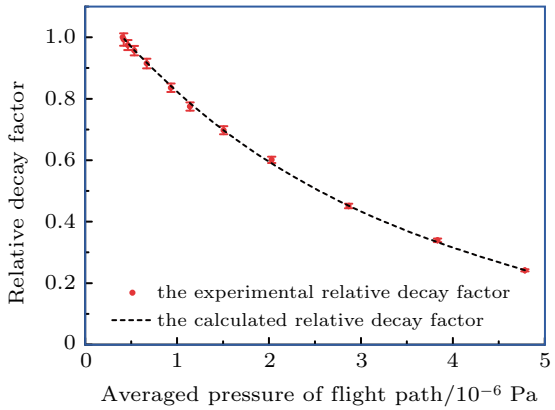



**Fig. 9.** (color online) Relative decay factor for cold atoms as a function of pressure. Red points show the experimentally measured values, and the black dash line shows the calculated relative decay factor due to the presence of residual gases.

As shown in the mass spectrum of Fig. 3, hydrogen is the main residual gas in the vacuum system. Table 1 shows that the coefficient between cold rubidium atoms and hydrogen is the largest one among the presented loss rate coefficients. Thus, we use it to estimate the required vacuum pressure. For cold atoms in microgravity environments, the lifetime of cold atoms limited by residual gases will be more than 10 seconds as the vacuum pressure is lower than $8.5 \times 10^{-8}$ Pa. If the vacuum pressure is lower than $2.85 \times 10^{-8}$ Pa, the lifetime of cold atoms limited by residual gases will be more than 30 seconds. In addition, cold atoms can be used as a vacuum pressure measurement tool according to the relationship between the loss of cold atoms and the vacuum pressure.[13,17,35]

## 5. Conclusion

We have experimentally and theoretically studied the loss rate of cold atoms due to collisions with residual gases in the MOT and during free flight. The mass spectrum is scanned by the residual gas analyzer under different vacuum environments, and the main residual gases are hydrogen, nitrogen, carbon monoxide, carbon dioxide, argon, and methane. We used the molecular flow module in COMSOL to obtain the partial pressure distribution for these main residual gases in the vacuum system. The relationship between the loss rate of cold atoms and several main residual gases were calculated. For the MOT loss rate, the contribution from background hot rubidium should be taken into account, and the loss rate agrees well with the calculated MOT loss rate. The agreement between the calculated and the measured loss rate of MOT also indicates that the results of the partial pressure distribution are credible. The measured relative decay factor during free flight under different vacuum pressures agrees well with the calculated relative decay factor obtained from semi-classical elastic scattering and the pressure distribution. Hence, it has been verified that the semi-classical elastic scattering is valid for the collision between cold atoms and residual gas during free flight. According to the semi-classical elastic scattering, we can quantify the loss of cold atoms caused by the residual gas and do further analyses of other mechanisms that lead to the loss of cold atoms.

## References

[1] Monroe C, Swann W, Robinson H and Wieman C 1990 *Phys. Rev. Lett.* **65** 1571
[2] Lindquist K, Stephens M and Wieman C 1992 *Phys. Rev. A* **46** 4082
[3] Santarelli G, Laurent Ph, Lemonde P, Clairon A, Mann A G, Chang S, Luiten A N and Salomon C 1999 *Phys. Rev. Lett.* **82** 4619
[4] Ramsey N F 1950 *Phys. Rev.* **78** 695
[5] Wang Q, Lin Y G, Li Y, Lin B K, Meng F, Zang E J, Li T C and Fang Z J 2014 *Chin. Phys. Lett.* **31** 123201
[6] Li W F, Du J J, Wen R J, Li G and Zhang T C 2015 *Chin. Phys. Lett.* **32** 104210
[7] Zhang F, Long Y, Yang J L, Ma G Q, Yin J P and Wang R Q 2015 *Chin. Phys. Lett.* **32** 123701
[8] Raab E L, Prentiss M, Cable A, Chu S and Pritchard D E 1987 *Phys. Rev. Lett.* **59** 2631
[9] Prentiss M, Cable A, Bjorkholm J E, Chu S, Raab E L and Pritchard D E 1988 *Opt. Lett.* **13** 452
[10] Bjorkholm J E 1988 *Phys. Rev. A* **38** 1599
[11] Bali S, O'Hara K M, Gehm M E, Granade S R and Thomas J E 1999 *Phys. Rev. A* **60** R29
[12] Van Dongen J, Zhu C, Clement D, Dufour G, Booth J L and Madison K W 2011 *Phys. Rev. A* **84** 022708
[13] Makhalov V B, Martiyanov K A and Turlapov A V 2016 *Metrologia* **53** 1287
[14] Simon E, Laurent P, Santarelli G, Clairon A, Lemonde P, Salomon C, Dimarcq N, Petit P, Audoin C, Gonzalez F and Changeart F J 1997 *Acta Astronautica* **40** 837
[15] Lü D S, Wang B, Li T and Liu L 2010 *Chin. Opt. Lett.* **8** 735
[16] Kulas S, Vogt C, Resch A, et al. 2017 *Microgravity Science and Technology* **29** 37

[17] Arpornthip T, Sackett C A and Hughes K J 2012 *Phys. Rev. A* **85** 033420

[18] Margenau H and Kestner N R 1971 *Theory of Intermolecular Forces* (New York: Pergamon Press)

[19] Miller J D, Cline R A and Heinzen D J 1993 *Phys. Rev. A* **47** R4567

[20] Vuletić V, Chin C, Kerman A J and Chu S 1998 *Phys. Rev. Lett.* **81** 5768

[21] Tollett J J, Bradley C C, Sackett C A and Hulet R G 1995 *Phys. Rev. A* **51** R22

[22] Monroe C R, Cornell E A, Sackett C A, Myatt C J and Wieman C E 1993 *Phys. Rev. Lett.* **70** 414

[23] Landau L D and Lifshits E M 1977 *Quantum Mechanics: Non-Relativistic Theory (Course of Theoretical Physics vol. 3)* (3rd Edn.) (New York: Pergamon Press)

[24] Child M S 1996 *Molecular Collision Theory* (New York: Courier Corporation)

[25] Cambi R, Cappelletti D, Liuti G and Pirani F 1991 *The Journal of Chemical Physics* **95** 1852

[26] Koutselos A D and Mason E A 1986 *The Journal of Chemical Physics* **85** 2154

[27] Ren W, Gao Y C, Li T, Lü D S and Liu L 2016 *Chin. Phys. B* **25** 060601

[28] Ren W, Xiang J F, Zhang Y T, Wang B, Qu Q Z, Zhao J B, Ye M F, Lü D S and Liu L 2015 *Vacuum* **116** 54

[29] Qu Q Z, Wang B, Lü D S, Zhao J B, Ye M F, Ren W, Xiang J F and Liu L 2015 *Chin. Opt. Lett.* **13** 061405

[30] Wang B, Lü D S, Qu Q Z, Zhao J B, Li T, Liu L and Wang Y Z 2011 *Chin. Phys. Lett.* **28** 063701

[31] Lü D S, Qu Q Z, Wang B, Zhao J B, Liu L and Wang Y Z 2011 *Chin. Phys. Lett.* **28** 063201

[32] Li L, Qu Q Z, Wang B, Li T, Zhao J B, Ji J W, Ren W, Zhao X, Ye M F, Yao Y Y, Lü D S and Liu L 2016 *Chin. Phys. Lett.* **33** 063201

[33] Haw M, Evetts N, Gunton W, Van Dongen J, Booth J L and Madison K W 2012 *J. Opt. Soc. Am. B* **29** 475

[34] Gensemer S D, Sanchez-Villicana V, Tan K Y N, Grove T T and Gould P L 1997 *Phys. Rev. A* **56** 4055

[35] Yuan J P, Ji Z H, Zhao Y T, Chang X F, Xiao L T and Jia S T 2013 *Appl. Opt.* **52** 6195